Journal of Pharmaceutical Sciences 105 (2016) 2129-2138

Contents lists available at ScienceDirect

Journal of Pharmaceutical Sciences

journal homepage: www.jpharmsci.org

Pharmaceutics, Drug Delivery and Pharmaceutical Technology

Ice Recrystallization in a Solution of a Cryoprotector and Its Inhibition by a Protein: Synchrotron X-Ray Diffraction Study

Boris Zakharov [1, 2], Alexander Fisyuk [3, 4], Andy Fitch [5], Yves Watier [5], Anastasia Kostyuchenko [3, 4], Dushyant Varshney [6], Michael Sztucki [5], Elena Boldyreva [1], Evgenyi Shalaev [7, *]

[1] Institute of Solid State Chemistry and Mechanochemistry SB RAS, ul. Kutateladze, 18, Novosibirsk 630128, Russian Federation
[2] Novosibirsk State University, ul. Pirogova, 2, Novosibirsk 630090, Russian Federation
[3] Department of Organic Chemistry, Omsk F. M. Dostoevsky State University, Mira Avenue 55A, Omsk 644077, Russian Federation
[4] Laboratory of New Organic Materials, Omsk State Technical University, Mira Avenue 11, Omsk 644050, Russian Federation
[5] ESRF—The European Synchrotron Radiation Facility, 71 av des Martyrs, Grenoble 38043, France
[6] Novartis Vaccines and Diagnostics, Holly Springs, North Carolina 27540
[7] Pharmaceutical R&D, Allergan Inc., Irvine, California 92612

ARTICLE INFO

Article history:
Received 30 December 2015
Revised 21 March 2016
Accepted 11 April 2016
Available online 7 June 2016

Keywords:
crystal defects
phase transition
proteins
calorimetry (DSC)
X-ray powder diffractometry
freeze drying/lyophilization

ABSTRACT

Ice formation and recrystallization is a key phenomenon in freezing and freeze-drying of pharmaceuticals and biopharmaceuticals. In this investigation, high-resolution synchrotron X-ray diffraction is used to quantify the extent of disorder of ice crystals in binary aqueous solutions of a cryoprotectant (sorbitol) and a protein, bovine serum albumin. Ice crystals in more dilute (10 wt%) solutions have lower level of microstrain and larger crystal domain size than these in more concentrated (40 wt%) solutions. Warming the sorbitol–water mixtures from 100 to 228 K resulted in partial ice melting, with simultaneous reduction in the microstrain and increase in crystallite size, that is, recrystallization. In contrast to sorbitol solutions, ice crystals in the BSA solutions preserved both the microstrain and smaller crystallite size on partial melting, demonstrating that BSA inhibits ice recrystallization. The results are consistent with BSA partitioning into quasi-liquid layer on ice crystals but not with a direct protein–ice interaction and protein sorption on ice surface. The study shows for the first time that a common (i.e., not-antifreeze) protein can have a major impact on ice recrystallization and also presents synchrotron X-ray diffraction as a unique tool for quantification of crystallinity and disorder in frozen aqueous systems.

Introduction

Freezing of aqueous solutions is a universal phenomenon in both the nature and various industrial processes used for pharmaceutical, food, and biotech products. In particular, many biopharmaceuticals are commonly stored in the frozen state or processed by freeze-drying to minimize degradation during shipping and storage. It was found that although rates of many physical and chemical processes decrease in the frozen state, freezing can also destabilize proteins[1,2] and actually increase rate of some chemical reactions including hydrolysis and oxidation.[3-6] Furthermore, the freeze-induced protein destabilization and increased chemical reactivity was shown to be related to ice formation per se rather than to low temperatures and freeze concentration.[7-10] Uncontrolled freezing and ice recrystallization can also lead to such undesirable events as major manufacturing losses during freeze-drying of pharmaceuticals due to vial breakage,[11,12] changes in texture, taste, and overall quality of frozen food, for example, ice cream,[13] and cryo-injury of cells and tissues.[14] Ice recrystallization can be influenced by certain solutes, in particular by antifreeze proteins.[15] In addition, purposeful ice recrystallization was shown to be beneficial for a freeze-drying process allowing acceleration of ice sublimation during manufacturing of freeze-dried pharmaceutical products[16,17] and also for improved protein stability by reducing fraction of proteins on interfaces.[18] The majority of studies

Current address for Dr. Varshney: Hospira, Inc., 275 North Field Drive Lake Forest, Lake Forest, Illinois 60045.
This article contains supplementary material available from the authors by request or via the Internet at http://dx.doi.org/10.1016/j.xphs.2016.04.020.
* *Correspondence to:* (Telephone: 714-246-3372).
E-mail address: shalaev_evgenyi@allergan.com (E. Shalaev).

http://dx.doi.org/10.1016/j.xphs.2016.04.020
0022-3549/

of ice recrystallization are performed with antifreeze proteins and their synthetic analogs.[19,20] Although "common" (i.e., not antifreeze) proteins are prevalent in pharmaceutical and food systems, their interaction with ice and their impact on ice recrystallization are studied in much lesser extent.

In studies of freezing behavior of aqueous systems, X-ray diffraction (XRD) represents a main experimental tool. XRD studies of aqueous solutions have been mainly focused on monitoring crystallization and polymorphism of solutes[21-24] and co-solvents,[25] whereas information obtained from the ice diffraction peaks is usually limited to qualitative aspects of freezing behavior, such as confirmation of freezing onset from the appearance of corresponding diffraction lines[26] and determination of the ice form, for example, hexagonal ("Ih") versus cubic ("Ic").[27,28] XRD has been also used to study interaction of antifreeze proteins and their synthetic analogs with specific faces of ice crystals, by monitoring disappearance of particular Ih diffraction peaks, for example, a peak corresponding to 002 diffraction plane.[29-31] Additional important information on recrystallization of frozen solutions could be obtained from the quantitative analysis of XRD data, by monitoring changes in the extent of crystallinity and microstrain in the crystalline lattice, such as lattice dislocations (linear defects) and stacking faults (planar defects). However, quantitative XRD analysis for frozen aqueous solutions is complicated by the preferred orientation effects, which necessitate additional sample treatment, such as grinding,[29] and also by instrumental broadening of diffraction lines. With the experimental setup of the present study, in which high-resolution X-ray powder diffraction beamline ID31 at the European Synchrotron Radiation Facility (ESRF) was used, such complications are greatly reduced,[32] allowing quantification of the amount of ice in "as is" samples without additional sample manipulation and evaluation of crystal disorder from the width of diffraction peaks. To the best of our knowledge, this work represents a first attempt to investigate freezing of aqueous solutions of pharmaceutically relevant solutes using quantitative XRD method, whereas application of XRD for quantitative analysis of powders has been reported previously.[33,34] In addition to XRD, differential scanning calorimetry (DSC) is used to measure the temperature ranges of the phase transitions and other physical transformations during cooling and warming of the solutions. In this article, binary aqueous solutions of 2 solutes, a polyhydroxy compound (sorbitol) and a protein (bovine serum albumin [BSA]), are studied. Sorbitol is a cryoprotector used to stabilize proteins and also a popular model system to study phase behavior and glass transition of polyhydroxy compounds. BSA is a "common" (i.e., non-antifreeze) protein, which is frequently used to study freezing and freeze-drying of protein solutions. Sorbitol 10, 40, and 60 wt% solutions and BSA 10 and 40 wt% solutions are selected for the study, to represent typical solute concentrations in pharmaceutically relevant samples (10 wt % concentration) and to evaluate impact of solute concentration on ice formation and recrystallization.

Experimental Methods

Sorbitol (>99.5% purity) and BSA (>98% purity) were obtained from Sigma-Aldrich. DSC analysis was performed with a Q2000 DSC system (TA Instruments). Nitrogen was used as purge gas, and calibration was performed using indium as the standard. Sorbitol and BSA solutions with target concentrations of 10 and 40 wt% of the solutes were prepared by dissolving weighed amounts of the reagents in deionized water. For each target concentration, 2 solutions were prepared independently, with actual concentrations of 9.95, 10.0, 40.1, and 40.7 wt% for sorbitol and 10.0, 10.4, 40.0, and 40.3 wt% for BSA. One solution (40.0 wt% BSA, first round) was sonicated to facilitate dissolution, whereas all other samples were prepared without sonication. Furthermore, 4 of these solutions (9.95 and 40.7 wt% sorbitol and 10.0 and 40.0 wt% BSA) were filtered using 0.2 μm PALL Acrodisc syringe filter. Overall, 3 sets of samples (2 unfiltered and 1 filtered) were tested by DSC. The solutions (~20 μL) were sealed in Tzero aluminum pans with hermetic lids, cooled to 193 K, and heated to 293 K with the scanning rate of 5 K/min. Three cooling/heating cycles were performed for each sample. Heterogeneous ice nucleation temperatures were determined from the onset of the exothermic event during cooling.

The high-resolution wide-angle XRD experiment was carried at the ESRF on the ID-31 beamline at the X-ray wavelength of 0.399962 ± 0.000014 Å. Solutions containing 10.0, 40.1, and 60.1 wt % sorbitol and 10.1 and 40.1 wt% BSA were prepared by dissolving weighed amounts of the solids in deionized water. The solutions were filled in 1.5-mm borosilicate glass capillaries and flash cooled by placing into cryostream of nitrogen gas with the temperature of 100 K for 30 min. The frozen samples were heated using the thermostat (cryostream) setting of 228 K (all samples but 60 wt% sorbitol) or 210 K (60 wt% sorbitol) with the gas heating rate of 360 K/h. The samples were equilibrated at corresponding temperatures for 30 min before measurements. The XRD intensities were sampled every 0.0005 degrees, which were then normalized and rebinned at appropriate steps (0.001, 0.01, 0.05 degree) depending on the widths of the peaks in the diffraction pattern, using in-house software id31sum.[35] At each temperature, at least 4 XRD measurements were performed from 0.1° to 93.95° 2θ, and the data were combined in a single averaged XRD pattern. For the background subtraction, an XRD scan of an empty capillary was carried out at 0.399844 ± 0.00006 Å wavelength, and the data were treated with smoothing and interpolation algorithm (using Topas) to the 0.05 degree binned data.

Results and Discussion

DSC Results

During cooling of solutions containing both 10 and 40 wt% of a solute, an exothermic peak of water crystallization is observed, as shown in Figure 1 (top) for 10 wt% sorbitol solution as an example. Secondary (eutectic) solute + water crystallization does not occur; therefore, these frozen solutions exist as a 2-phase mixture of crystalline water (ice) and an amorphous freeze-concentrated solution. Ice nucleation temperatures are provided in Table 1. Note that ice nucleus is likely formed on the solution–container interface or on solid particles, that is, via heterogeneous nucleation mechanism. Particles, which can serve as ice nucleus, are always present in any solution unless a special sample preparation and handling procedure is used, such as dividing a solution into a large number of small droplets (typically $>10^6$ droplets for sample size of a few microliters[37-39]) so that the majority of droplets remain particle free. Homogeneous ice nucleation temperature for water is approximately 235 K,[40] whereas the ice nucleation temperature for the water samples in this study is higher (see Table 1), as expected.

For sorbitol solutions, an increase in the solute concentration from 10 to 40 wt% lowers both ice nucleation and equilibrium melting temperatures (Table 1), which is consistent with the behavior for other low–molecular weight solutes.[41-43] Relationship between equilibrium ice melting point (water liquidus) and T_{het} is described by Equation 1[41]:

$$\Delta T_{het} = k\,\Delta T_m \quad (1)$$

where ΔT_{het} is the reduction of the temperature of heterogeneous nucleation associated with the addition of a solute, ΔT_m is the freezing point depression, and k is an empirical constant.

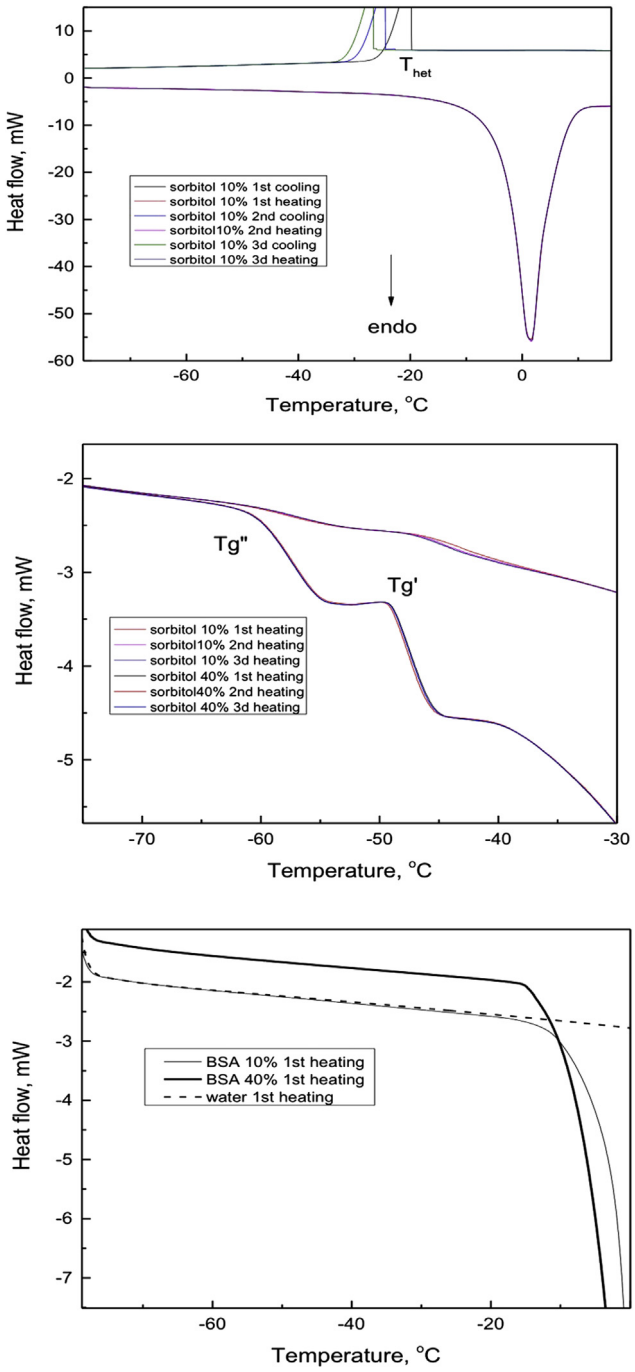

Figure 1. DSC curves obtained during cooling/warming of 10 wt% sorbitol solution (top), during warming of 10 and 40 wt% sorbitol solutions (middle), and during warming of 10 and 40 wt% BSA solutions and water (bottom). For BSA solutions, second and third heating curves were essentially identical, and they are not shown.

k depends on the nature of both heterogeneous nucleus and the solute and was found to be between 1.5 and 4.4[42] and 1.3 to 2.6[43] with different combinations of solutes and nucleation agents. Note that a similar expression has been introduced earlier to describe relations between the equilibrium melting point and homogeneous ice nucleation temperature,[37,39] although the *k* values for homogeneous ice nucleation are typically smaller, between 1 and 2. For sorbitol solutions, *k* is determined to be 2.4 from the data presented in Table 1, which is within the range reported in the literature[42,43] for other solutes.

The results of Table 1 point out to 2 potentially interesting observations. First, there is no systematic difference between filtered and nonfiltered samples, whereas, from the general perspectives, filtered samples could be expected to have lower ice nucleation temperatures on account of a reduced concentration of potential centers of heterogeneous nucleation. This somewhat unexpected result could imply that either ice nuclei are formed on solution–container interface or the size of a heterogeneous nucleus is smaller than the filter cut-off size of 0.2 μm. Separately, there is a difference in the heterogeneous ice nucleation temperatures between sorbitol and BSA solutions, with sorbitol solutions freezing at lower temperatures. It should be stressed, however, that these findings should be considered as preliminary observations because studies of such probabilistic process as nucleation would require much larger statistics, with tens and hundreds of replicates,[44] as well as a control of the type and concentration of centers of heterogeneous nucleation. In addition, ice nucleation temperature could also depend on the sample volume; therefore, ice nucleation temperatures as measured by DSC would probably be not the same as freezing temperatures of real pharmaceutical products.

Magnified parts of DSC heating curves for sorbitol and BSA solutions are shown in Figure 1 (middle) and Figure 1 (bottom), respectively. For sorbitol–water samples, 2 endothermic steps, commonly called *Tg″* and *Tg′*, followed by ice melting endotherm, are observed. Although such DSC curves are typical for aqueous solutions of polyhydroxy compounds and other amorphous solutes, the interpretation of the physical nature of these 2 events is still controversial and is a subject of numerous publications,[45-54] as summarized subsequently. The lower temperature event (so-called *Tg″*) has been commonly attributed to the glass transition of the freeze concentrate, although there is still some disagreement whether it represents maximally freeze-concentrated solution. The second event (*Tg′*) is proposed to be due to either the onset of ice melting/dissolution in the freeze-concentrated solution[48,52] or a glass transition of the maximally freeze-concentrated solution.[47,49] Interpretation of the freeze-thaw behavior of aqueous systems (such as citric acid and sucrose) has been refined recently using an optical cryo-microscopy and DSC.[55,56] In particular, it has been proposed that freeze-concentrated solutions have 2 concentration regions, FCS_1 (maximally freeze-concentrated solution) and FCS_2, which has a lower solute (and higher water) concentration than FCS_1. Furthermore, it has been shown that ice formation, which is incomplete during cooling, re-starts during warming when the sample temperature approaches the glass transition temperature of FCS_2. Therefore, the thermal event which is commonly called *Tg′* (Ttr_2 in Bogdan et al.[56]) could be due to re-start of ice crystallization in the FCS_2 region and simultaneous glass-to-liquid transition in FCS_1. Although physical mechanisms behind the existence of freeze-concentrated regions with different solute concentrations have not been established, a hypothesis has been presented recently. According to this hypothesis, volume expansion during water-to-ice transformation could cause an increase in the local pressure in some locations of a particular sample, which in turn would change the water liquidus and, therefore, composition of the freeze-concentrated solution.[57,58]

For BSA–water mixtures (Fig. 1, bottom), DSC heating curves show a broad ice-melting endotherm with an onset at approximately 255 K, whereas neither *Tg′* nor *Tg″* were observed. This is consistent with previous reports (e.g., Gekko and Satake[59]) on DSC studies of protein–water mixtures. The lack of any glass transition thermal events for the freeze-concentrated solution BSA could be because proteins represent so-called strong glasses with a very small heat capacity change at the glass-to-liquid transition.[60]

Table 1
Heterogeneous Ice Nucleation Temperatures from DSC Experiments and Water Liquidus Temperatures

Sample	Heterogeneous Ice Nucleation Temperature (°C) Average ± SD				Liquidus Temperature (Equilibrium Melting Point) (°C)
	Unfiltered, First Round	Unfiltered, Second Round	Filtered, Second Round	Average	
Water	−13.4 ± 1.4	−17.1 ± 1.3	−11.7 ± 0.3	−14.1 ± 2.6	0.0
10 wt% Sorbitol	−23.5 ± 2.7	−20.8 ± 5.2	−24.1 ± 0.2	−23.1 ± 3.3	−0.9[a]
40 wt% Sorbitol	−37.6 ± 0.5	−29.7 ± 0.5	−30.2 ± 0.7	−32.5 ± 3.9	−6.5[a]
10 wt% BSA	−7.3 ± 0.1	−19.1 ± 2.0	−18.2 ± 0.5	−14.9 ± 5.8	0[b]
40 wt% BSA	−21.1 ± 1.1	−18.5 ± 2.2	−17.0 ± 0.6	−18.9 ± 2.2	0[b]

[a] From the water–sorbitol phase diagram (Supplementary Data).
[b] From interpolation of the data reported in Panagopoulou et al.[36]

XRD Results—10 Wt% Sorbitol

XRD patterns of 10 wt% solutions of sorbitol and BSA at 100 K are shown in Figure 2, along with the theoretical pattern of Ih.[61] The peaks in either pattern are consistent with Ih, although several additional weak diffractions are detected in the vicinity of peaks corresponding to *hkl* 105, 006, 205, 310, and 215. Although the origin of these additional peaks is not known, we note that a "splitting" of ice peaks, that is, observation of ≥2 peaks instead of a single ice peak was reported earlier and attributed to the deformation of ice crystal lattice and the corresponding change of lattice parameters during freezing.[58] These additional weak peaks are included in the consecutive data analysis. In addition to the ice peaks, an amorphous halo is observed as well (Fig. 3 insert), indicative of a 2-phase system consisting of Ih and an amorphous freeze-concentrate containing sorbitol and unfrozen water. At 228 K, the XRD pattern is qualitatively similar to the 100 K pattern, with both Ih peaks and amorphous halo detected. The Ih peaks are shifted to lower diffraction angles (higher d-spacing) compared with the pattern at 100 K, as expected. A quantitative analysis of the XRD data is performed to investigate changes in ice crystals on heating from 100 to 228 K. As the first step, changes in the relative amount of ice crystals after heating are evaluated, by quantifying both the diffraction intensity from the ice crystals and total diffraction of ice plus amorphous halo from the freeze-concentrated solution.

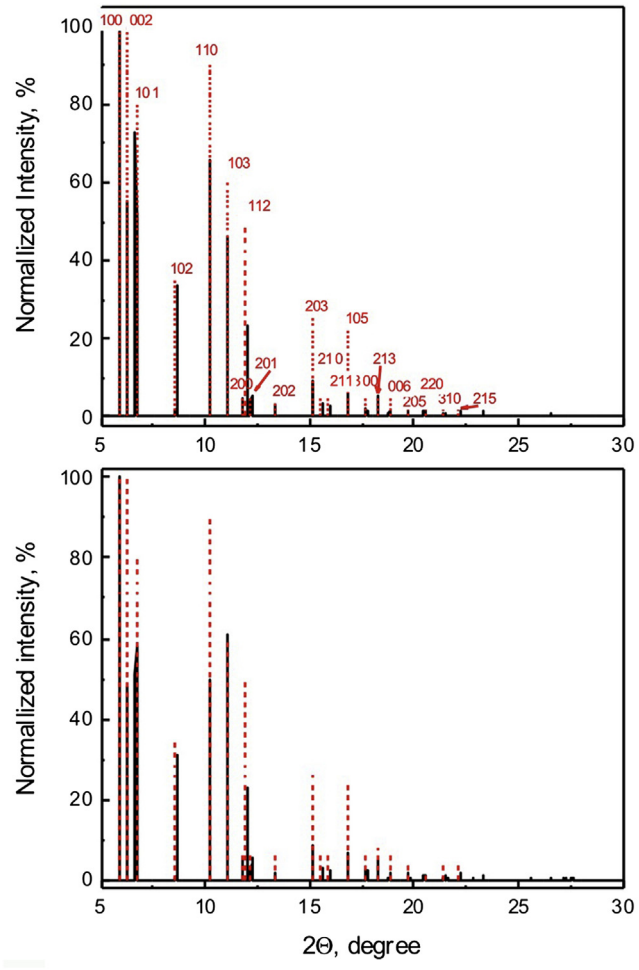

Figure 2. XRD patterns of 10 wt% solutions of sorbitol (top) and BSA (bottom) at 100 K, normalized to the intensity of diffraction peak corresponding to *hkl* 100. Theoretical pattern of hexagonal ice at 90 K is shown as red dashed lines.

Specifically, 2 integrations are performed for each XRD pattern in the 2θ region from 5° to 25°. In the first integration, both amorphous halo and all crystalline peaks are included, whereas only crystalline peaks are integrated in the second integration (an example is provided in the Supplementary Data). As a first approximation, the weight fraction of ice, x_1, can be calculated as

$$x_1/(x_1 + x_2) = I_1/(I_1 + I_2) \quad (2)$$

where I is the integrated intensity of the diffractions, subscripts 1 and 2 correspond to ice and freeze-concentrated solution, respectively, and $x_1 + x_2 = 1$.

It should be noted that although the diffraction intensity is proportional to the amount of a particular phase present, it also depends on other factors, that is, the mass absorption coefficient (or mass attenuation coefficient, with 2 terms used interchangeably[62]) and density, and also on the geometry of an XRD instrument and selection of a particular plane (*hkl*) for data analysis,[63]

$$I_i = K_i x_i / \{\rho_i [x_i(\mu_i^* - \mu_m^*) + \mu_m^*]\} \quad (3)$$

where K_i is a coefficient which depends on the nature of the component I, selected plane (*hkl*), and the geometry of the XRD apparatus, ρ_i is density, μ^* is mass absorption coefficient, and i and m correspond to the component I and matrix, respectively.

To account for the additional variables (Eq. 3) in the calculations of the crystallinity from the XRD data, Equation 4 is derived as described in the Supplementary Data.

$$x_2/x_1 = C(I_2/I_1)(\rho_2/\rho_1) \quad (4)$$

where an empirical coefficient C is determined to be equal to 0.89 ± 0.01 (see the Supplementary Data for determination of the C value).

Equation 4 is also used to calculate a relative change in the ice fraction on heating from 100 to 228 K, Δx_1,

$$\Delta x_1 = 100 \times (x_{1,100K} - x_{1,228K})/x_{1,100K} \quad (5)$$

The x_1 and Δx_1 values obtained from Equations 2 and 4 (x_1) and Equation 5 (Δx_1) are presented in Table 2. The decrease in

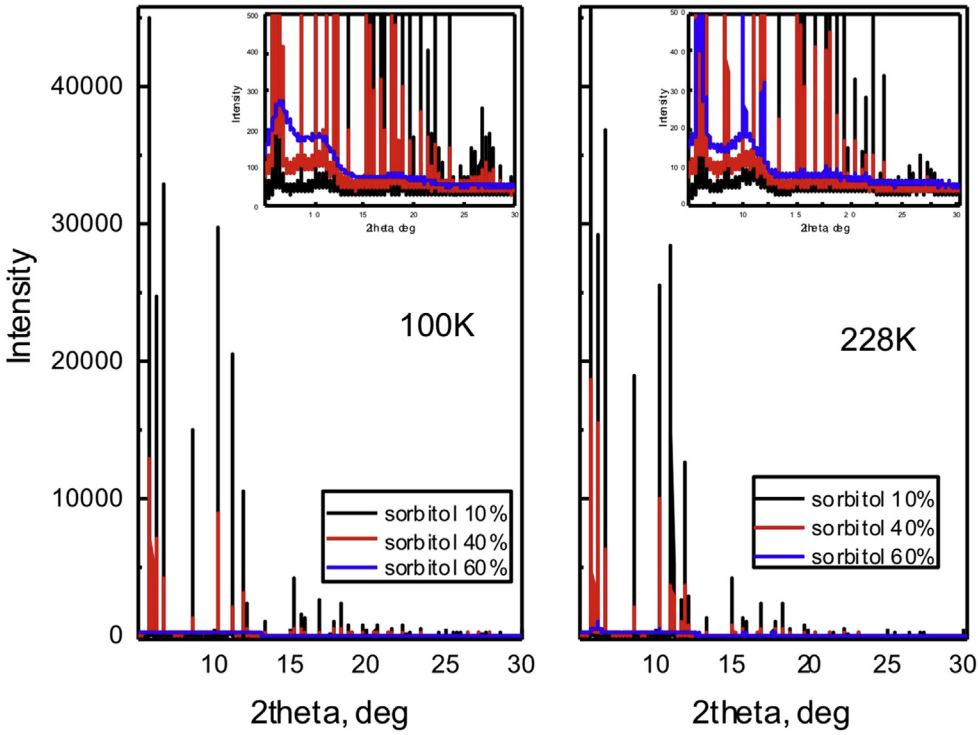

Figure 3. XRD patterns of sorbitol–water mixtures at 100 K (left) and 228 K (right). Note that the pattern for 60 wt% sorbitol on the right graph was obtained at 210 K. Inserts present magnified portions of the patterns showing amorphous halo. A.U, arbitrary units.

crystallinity, which is estimated directly from the diffracted intensities using Equation 2 (i.e., without corrections for the densities and mass absorption coefficients), is similar to the refined value for 10 wt% sorbitol (15% directly from the diffracted intensities vs. 19% with corrections). Therefore, heating 10 wt% sorbitol sample from 100 K to the thermostat temperature of 228 K results in a partial melting of ice crystals, with the corresponding reduction in crystallinity of approximately 15%-20% as related to the initial crystallinity at 100 K.

Furthermore, ice fraction in the 10 wt% sorbitol–water frozen mixture is calculated from the water–sorbitol phase diagram[64] (Supplementary Data) using the lever rule[65] and also provided in Table 2. Ice weight fraction value, which is obtained from the XRPD data at 100 K (0.84 or 0.87 according to Eq. 2 or Eq. 4, respectively), is reasonably close to that calculated from the phase diagram of sorbitol–water system (0.88). At 228 K, however, the experimentally measured ice fraction is significantly lower than the theoretical value. Two factors can be responsible for the discrepancy between the experimental and theoretical values, that is, a difference between the thermostat set-point and the actual sample temperature during the experiment due to the temperature gradient between the heat-transfer gas media and the sample and irradiation-induced ice melting. In particular, X-ray exposure could result in local heating due to radiation absorption during the data collection. For example, a substantial (4-23 K) increase in the temperature has been observed in synchrotron X-ray radiation experiments.[66] In addition, irradiation-induced pre-melting of ice on ice–silica interfaces has been reported and attributed to the increase in ionic defects in ice, mainly due to interaction of the secondary electrons with ice by inelastic scattering.[67] It is possible (and indeed likely) that the decrease in the amount of ice observed in this study on heating from 100 K to the thermostat temperature of 228 K is due to a combination of these 2 effects, that is, the local radiation heating during the data collection and irradiation-induced ice melting.

Table 2
Fraction of Ice in Sorbitol–Water and BSA–Water Systems Obtained From the XRD Data and the Theoretical Values Obtained From Sorbitol–Water Phase Diagram[64] (see Supplementary Data for Details of Theoretical Calculations)

Sample	Thermostat Temperature	Weight Fraction of Ice in Frozen Solution, x_I			Decrease in the Ice Fraction at 228 K as a % of 100 K Data		
		Theoretical	From Equation 2	From Equation 5	Theoretical	From Equations 2 and 5	From Equations 4 and 5
Sorbitol 10 wt%	100 K	0.88	0.87	0.84	1.1	14.9	19.0
	228 K	0.87	0.74	0.68			
Sorbitol 40 wt%	100 K	0.51	0.63	0.55	7.8	9.5	9.1
	228 K	0.47	0.57	0.50			
Sorbitol 60 wt%	100 K	–	0	0	–	–	–
	210 K	0.26	0.26	0.21			
BSA 10 wt%	100 K	–	0.88	0.86	–	15.9	18.6
	228 K	–	0.74	0.70			
BSA 40 wt%	100 K	–	0.66[a]	0.61[a]	–	10.0	9.8
	228 K	–	0.60	0.55			

[a] The maximum ice mass fraction is 0.6 based on the water content of 60 wt% (40 wt% BSA).

XRD Results—40 Wt% and 60 Wt% Sorbitol and 10 Wt% and 40 Wt% BSA

Similar to 10 wt% sorbitol solution, only Ih and amorphous phase are detected in 10 wt% BSA and both 40 wt% solutions. Positions of the ice peaks are the same between all 4 samples, whereas the intensities of the ice peaks are lower and the amorphous halo is more pronounced in more concentrated 40 wt% solutions (Figs. 3 and 4). Furthermore, the Ih fraction is calculated from the XRD data as described earlier, and the results are provided in Table 2. A similar reduction in the amount of ice after heating from 100 K to the thermostat temperature of 228 K is observed between sorbitol and BSA samples, with decrease in crystallinity of approximately 10% (for more concentrated solutions) and 15% to 20% (more dilute solutions). Note that, for BSA solutions, ice melting is expected to commence >250 K based on the DSC data (Fig. 1); therefore, actual temperature of the ice−solution interface in the samples exposed to the X-ray beam is probably higher than the thermostat temperature of 228 K, as also discussed earlier for the 10 wt% sorbitol solution.

Very different behavior is observed for 60 wt% sorbitol solution, which remained amorphous after cooling to 100 K, whereas ice is formed after warming to 210 K. The hindrance of ice formation during cooling of highly concentrated solutions is usually attributed to their high viscosity and liquid-to-glass transformation, although an alternative hypothesis has been introduced recently.[68] Heating the amorphous 60 wt% sorbitol solution to 210 K results in the appearance of crystalline lines (Fig. 3, right, insert), and the XRD pattern is consistent with the presence of cubic ice (Ic), showing greater intensity of the peak centered at approximately 6.2° 2θ, which corresponds to both 002 diffraction of Ih and 111 diffraction of Ic. Although such behavior is typical for concentrated solutions of monosaccharide and disaccharide,[28,69] this is probably the first report of observation of Ic in a solution of a sugar alcohol. Recently, a refined interpretation of such XRD patterns was proposed, introducing stacking-disordered ice in which cubic and hexagonal stacking sequences are randomly arranged.[70]

XRD—Line Broadening

An information about the extent of disorder in the crystalline phase (i.e., Ih in this case) can be obtained from line broadening. There are several contributions to peak broadening, including instrumental effect (which is negligible for ID31 beamline used in this study[32]) and any lattice imperfections, which can be further divided into crystalline size, and microstrains such as lattice dislocations (linear defects) and stacking faults (planar defects).[71] To evaluate impact of solute type, concentration, and temperature on line broadening, full width at half maximum (FWHM) values are obtained for each peak in the range of 5-25° 2θ, using peak analysis function of OriginPro software, version 9.1. The FWHM data are presented in Figure 5 as a function of diffraction angle. Figure 5 demonstrates that the concentration dependence of the peak width is qualitatively similar for BSA and sorbitol samples, with broader peaks observed for 40 wt% solutions, as could be expected due to a higher viscosity of the more concentrated solutions. As also shown in Figure 5, diffraction angle dependence of the FWHM is observed, indicative of a major strain-relative broadening,[72] although crystalline size broadening cannot be ruled out and, indeed, probably contributing to the peak broadening as well, as shown subsequently. A major difference in the temperature-induced changes in the peaks broadening of the sorbitol versus BSA solutions should be stressed. For sorbitol samples, peaks at the thermostat temperature of 228 K are narrower than at 100 K (Fig. 5) for both 10 and 40 wt% solutions, indicative of reduction in strains in crystal lattice and/or increase in crystalline domain size. In BSA solutions, from the other hand, the FWHM does not change (40 wt% solution) or even increases (10 wt% solution) on heating.

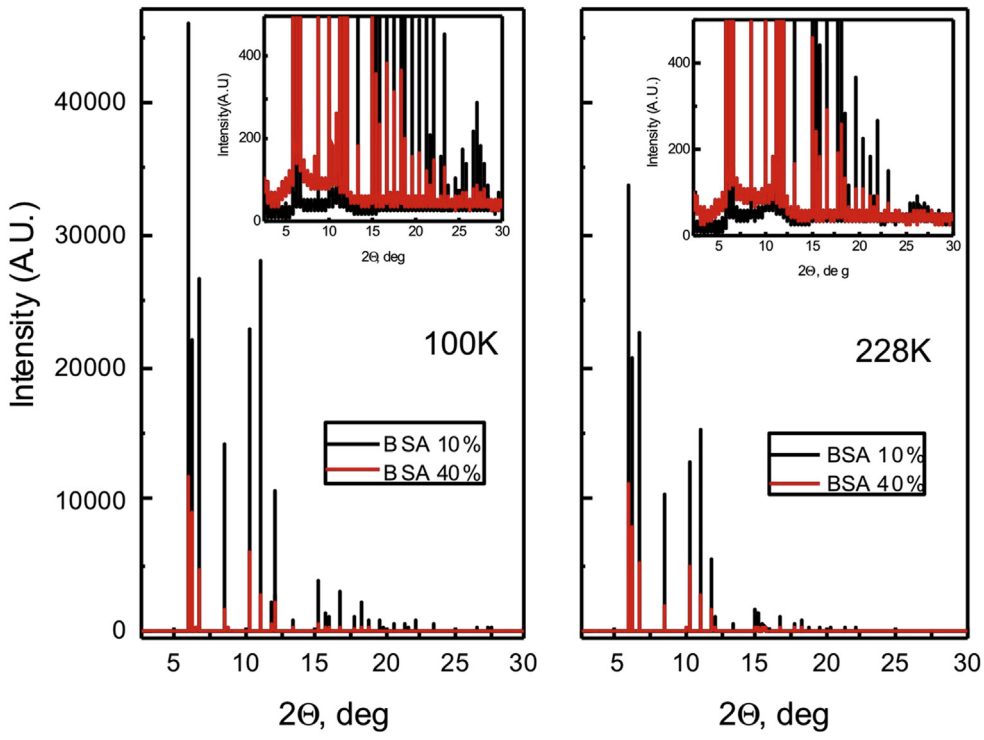

Figure 4. XRD patterns of BSA−water mixtures at 100 K (left) and 228 K (right). Inserts present magnified portions of the patterns showing amorphous halo. A.U., arbitrary units.

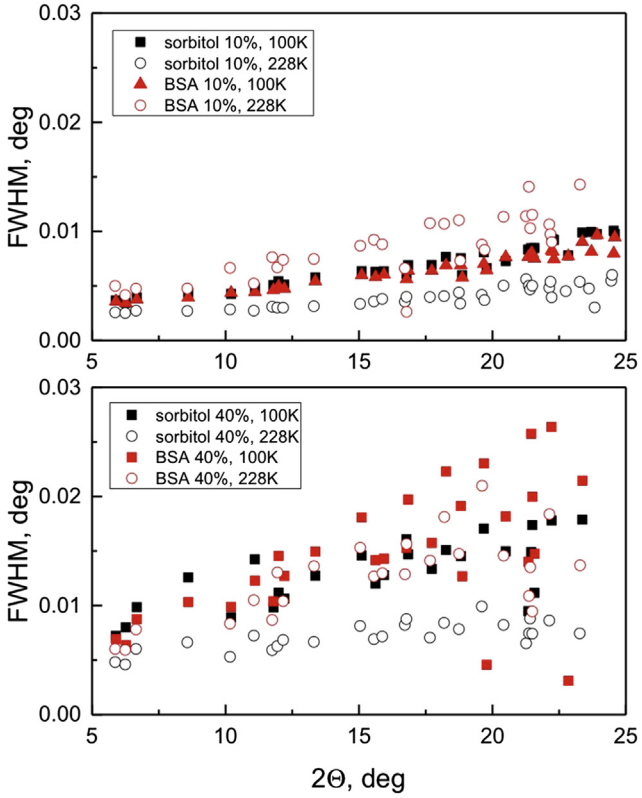

Figure 5. Diffraction angle dependence of the FWHM of the ice XRD peaks for 10 wt% solutions (top) and 40 wt% solutions (bottom).

Contributions from the finite crystalline size and microstrain to the peak broadening can be distinguished from Williamson–Hall (WH) plot analysis[73]

$$\beta^2 = \left(\frac{\lambda}{D\cdot\cos(\theta)}\right)^2 + (4\cdot\varepsilon\cdot tg(\theta))^2 \quad (6)$$

where β is a peak broadening (FWHM), λ is wavelength, D is coherent scattering length caused by size of individual crystallites (i.e., the size of crystalline domains), θ is a diffraction angle, and ε is a strain component which is caused by defect structure of individual crystallites.

Note that D, the size of crystalline domains, is not generally the same as the particle size, due to the presence of grain boundaries and polycrystalline aggregates. Lattice strain, ε, is a measure of the distribution of lattice constants arising from crystal imperfections, such as lattice dislocation and stacking faults. The dependence between $(\beta^2) \times (\cos(\theta))^2$ and $(\sin(\theta))^2$ is plotted and linearized using OriginPro software (graphs are shown in Supplementary Data), and $(4\ \varepsilon)^2$ and $(\lambda^2)/(D^2)$ are obtained from the slope and the intercept values, respectively. D and ε values, which are obtained from the WH plots, are presented in Table 3.

According with the results from the WH plot analysis (Table 3), 40 wt% sorbitol solution at 100 K has significantly smaller ice crystallite size than 10 wt% solution (43 vs. 186 Å). The microstrain is also higher than in less concentrated 10 wt% solution, although the difference is within the uncertainty. The same trend is observed for BSA solutions at 100 K, with smaller crystallite size (48 vs. 159 Å) and a higher strain for the more concentrated solution. Furthermore, heating to the thermostat temperature of 228 K results in a significant increase in the crystallite size and decrease in strain for both 10 and 40 wt% sorbitol solutions. This observation of

Table 3
Ice Crystallite Size, D, and Microstrain, ε, Obtained From the WH Plot Analysis

Sample	Thermostat Temperature	$D \pm$ SE (Å)	$\varepsilon \pm$ SE ($\times 10^3$)
Sorbitol 10 wt%	100 K	186 ± 23	10.9 ± 2.5
	228 K	198 ± 16	5.5 ± 1.9
Sorbitol 40 wt%	100 K	43.4 ± 2.2	16.6 ± 7.7
	228 K	69.9 ± 2.3	7.8 ± 3.8
BSA 10 wt%	100 K	159 ± 12	9.7 ± 2.3
	228 K	128 ± 31	13.9 ± 5.5
BSA 40 wt%	100 K	48.3 ± 8.1	22.8 ± 12.2
	228 K	46.6 ± 4.3	17.1 ± 9.5

simultaneous reduction in ice fraction (i.e., partial melting) and increase in crystallite size and decreased strain is consistent with recent studies of relevant aqueous systems containing small-molecular weight solutes,[57] which reported that ice melting occurred at the same time as recrystallization. This partial melting/recrystallization process can be expected to produce larger crystals with lower concentration of defects, which is indeed observed for sorbitol solutions in this study. However, the opposite trend is observed for BSA solutions, as shown in Figure 5, which compares the width of ice XRD peaks in sorbitol versus BSA solutions at 2 temperatures. Although heating of the sorbitol samples results in more narrow ice peaks (open vs. closed black symbols in Fig. 5), BSA solutions have broader (10 wt%) or similar (40 wt%) FWHM at 228 K (Fig. 4). Furthermore, the WH analysis (Table 3) shows no increase in crystalline size on heating for BSA samples, that is, no ice recrystallization, in contrast with the sorbitol solutions. Overall, the FWHM results demonstrate that although ice recrystallization takes place in sorbitol solutions, BSA inhibits ice recrystallization.

Protein–Ice Interaction

The majority of studies on protein–ice interactions are performed with antifreeze proteins and their synthetic analogs. Therefore, it would be appropriate to refer to the findings from these reports, at the same time recognizing that the analogy is not perfect, in part because concentration of antifreeze proteins is usually lower than the BSA concentrations used in this study.

Among several different types of antifreeze activities, 2 are particularly relevant to this study, that is, dynamic ice shaping (DIS) and ice recrystallization inhibition.[74] Inhibition of ice recrystallization by antifreeze proteins is related to their interference with the Ostwald ripening. For example, smaller ice crystals were found in aqueous solutions of specially designed antifreeze block copolymers, and the ice crystals retained their original size and morphology (suppressed Ostwald ripening) even after long growth times.[75] Broadening of XRD peaks by antifreeze polymers was also reported.[29] Although the exact mechanisms of inhibition of ice recrystallization by antifreeze proteins has not been established, it has been proposed that it is related to their partitioning to and interaction with the quasi-liquid layer on the surface of ice crystals, where the antifreeze molecules are competing with growing ice crystals for water molecules.[74,75] Quasi-liquid layer (also known as liquid-like layer) is a thin film of liquid water on the surface of ice crystals, which exists below the ice melting temperature.[76] Estimations of the thickness of the layer vary widely, from a few angstroms to up to a micometer.[77] By extending the hypothesis on antifreeze protein–quasi-liquid layer interaction to this investigation, we propose that the inhibition of ice recrystallization by BSA can be caused by the partitioning of BSA molecules into the quasi-liquid layer present on ice surface.

The DIS is due to a selected inhibition of the growth of certain crystalline faces and can be monitored by XRD as elimination

Table 4
Comparison of Expected XRD Results Under 2 Hypothetical Scenarios for Protein–Ice Interaction With the Experimental Observations for BSA Solutions

Expected Experimental Outcomes	Hypothetical Physical Mechanism 1: Protein Sorption on Ice Crystal (Direct Protein–Ice Interaction)	Hypothetical Physical Mechanism 2: Protein Partitioning into the Liquid Layer on Ice–Solution Interface	Experimental Observations for BSA Solutions
Outcome 1: Absence of some of Ih peaks in the X-ray diffractogram (consequence of a DIS)	Yes	No (i.e., all peaks are present)	No (i.e., all peaks are present)
Outcome 2: No increase in Ih crystallite size and no reduction in microstrain (consequence of inhibition of ice recrystallization)	Yes	Yes	Yes

(absence) of specific peaks, most commonly 002 peak.[31] Many antifreeze proteins inhibit growth of ice crystals by preferentially interacting with prism faces of ice crystals and, thus, inhibiting ice crystal growth in corresponding directions.[78] BSA does not show any signs of DIS because all the Ih peaks are present in the XRD patterns (Fig. 4). This is consistent with Raymoind and DeVries,[79] in which a major change in crystal habit was observed with antifreeze proteins but not with BSA. Therefore, the lack of DIS for BSA suggests that this protein does not bind selectively to a specific face of hexagonal ice.

To summarize, there are 2 alternative scenarios for protein–ice interaction, which would provide different XRD outcomes. These 2 scenarios are compared with the experimental observations for BSA solutions in Table 4. The XRD results are consistent with BSA partitioning into and interacting with the quasi-liquid layer but not with a direct protein sorption on ice crystals.

It should be also added that while sorption of antifreeze proteins on ice–solution interface has being observed experimentally,[80] there are no direct confirmations of such ice–protein interaction for pharmaceutically relevant proteins. Indeed, although reports of higher protein concentration on the surface of freeze-dried cake[81,82] are consistent with protein sorption on ice crystals during freezing, an alternative explanation is also available. It has been proposed that an increase in air–solution interface during freezing (due to formation of air bubbles by ice crystallization front), and sorption of proteins on these newly formed air–solution interfaces, could also be invoked to explain the increased protein surface concentration.[57] Similarly, freeze-induced destabilization of proteins[2,83] could be explained by both protein sorption on ice crystals and protein sorption on air–solution interface due to air bubbles formed during freezing.

Conclusions

Synchrotron XRD is used to evaluate extent of crystallinity and disorder of ice crystals during cooling and subsequent warming of aqueous solutions of sorbitol and BSA. Ice crystals, which are formed during cooling of more dilute (10 wt%) solutions, have lower microstrain and larger crystal size than these observed in more concentrated (40 wt%) solutions. Recrystallization of ice, that is, increase in the crystallite size and reduction in microstrain, is observed during warming of sorbitol solutions. The recrystallization takes place in parallel with decrease in the intensity of ice peaks and reduction of crystallinity by approximately 10-20 relative %, indicative of preferential dissolution–melting of the smaller ice crystals and these with the higher strain levels. BSA solutions, from the other hand, show opposite trend, with ice crystal disorder remaining and even increasing on partial melting. Based on the retention of all peaks of Ih in BSA solutions (i.e., the absence of DIS activity), BSA molecules are not preferentially sorbed on a particular face of growing ice crystal. This conclusion is consistent with an earlier publication, in which BSA did not have any impact on the interfacial energy on ice–solution interface,[84] whereas surface sorption, as in case on antifreeze proteins, usually results in a significant lowering of the interfacial energy. Considering the 2 experimental observations, that is, inhibition of recrystallization of ice crystals and the absence of DIS activity, and also on findings from literature on antifreeze proteins, we suggest that BSA molecules are partitioned into quasi-liquid layer present on ice crystals, whereas the question about a direct protein–ice interaction and protein sorption on ice surface remains open. Overall, this investigation demonstrates that synchrotron XRD is a powerful tool to study ice recrystallization and solute–ice interaction in pharmaceutical solutions and also highlights the need to address specific aspects of such measurements, such as the need to account for and minimize radiation-induced local heating. In a follow-up study, we are planning to further develop and apply this approach to a wider range of systems of pharmaceutical interest, including proteins and cryoprotectors.

Acknowledgments

The study was supported via ESRF proposal LS-2228. The authors thank 4 anonymous reviewers for valuable comments and suggestions.

References

1. Singh SK, Nema S. Freezing and thawing of protein solutions. In: Jameel F, Hershenson S, eds. *Formulation and Process Development Strategies for Manufacturing Biopharmaceuticals*. Hoboken, NJ: John Wiley & Sons, Inc.; 2010: 625-675.
2. Bhatnagar BS, Bogner RH, Pikal MJ. Protein stability during freezing: separation of stresses and mechanisms of protein stabilization. *Pharm Dev Technol*. 2007;12:505-523.
3. Lund DB, Fennema OR, Powrie WD. Enzymic and acid hydrolysis of sucrose as influenced by freezing. *J Food Sci*. 1969;34:378-382.
4. Pincock RE, Kiovsky TE. Kinetics of reactions in frozen solutions. *J Chem Educ*. 1966;43:358-360.
5. Pincock RE. Reactions in frozen systems. *Acc Chem Res*. 1969;2:97-103.
6. Takenaka N, Bandow H. Chemical kinetics of reactions in the unfrozen solution of ice. *J Phys Chem*. 2007;111:8780-8786.
7. Franks F, Hatley RHM. Stability of proteins at subzero temperatures: thermodynamics and some ecological consequences. *Pure Appl Chem*. 1991;63:1367-1380.
8. Schwegman JJ, Carpenter JF, Nail SL. Evidence of partial unfolding of proteins at the ice/freeze-concentrate interface by infrared microscopy. *J Pharm Sci*. 2009;98:3239-3246.
9. Bhatnagar BS, Pikal MJ, Bogner RH. Study of the individual contributions of ice formation and freeze-concentration on isothermal stability of lactate dehydrogenase during freezing. *J Pharm Sci*. 2008;97:798-814.
10. Anzo K, Harada M, Okada T. Enhanced kinetics of pseudo first-order hydrolysis in liquid phase coexistent with ice. *J Phys Chem A*. 2013;117:10619-10625.
11. Milton N, Gopalrathnam G, Craig GD, Mishra DS, Roy ML, Yu L. Vial breakage during freeze-drying: crystallization of sodium chloride in sodium chloride-sucrose frozen aqueous solutions. *J Pharm Sci*. 2007;96:1848-1853.
12. Williams NA, Dean T. Vial breakage by frozen mannitol solutions: correlation with thermal characteristics and effect of stereoisomerism, additives, and vial configuration. *J Parenter Sci Technol*. 1991;45:94-100.

13. Regand A, Goff HD. Effect of biopolymers on structure and ice recrystallization in dynamically frozen ice cream model systems. *J Dairy Sci*. 2002;85:2722-2732.
14. Baust JM, Van Buskirk R, Baust JG. Cell viability improves following inhibition of cryopreservation-induced apoptosis. *In Vitro Cell Dev Biol Anim*. 2000;36:262-270.
15. Davies PL. Ice-binding proteins: a remarkable diversity of structures for stopping and starting ice growth. *Trends Biochem Sci*. 2014;39:548-555.
16. Randolph TW, Searles JA. Freezing and annealing phenomena in lyophilization: effects upon primary drying rate, morphology, and heterogeneity. *Am Pharm Rev*. 2002;5, 40,42,44-46.
17. Hottot A, Vessot S, Andrieu J. Freeze drying of pharmaceuticals in vials: influence of freezing protocol and sample configuration on ice morphology and freeze-dried cake texture. *Chem Eng Process*. 2007;46:666-674.
18. Xu Y, Grobelny P, Von Allmen A, et al. Protein quantity on the air—solid interface determines degradation rates of human growth hormone in lyophilized samples. *J Pharm Sci*. 2014;103:1356-1366.
19. Hassas-Roudsari M, Goff HD. Ice structuring proteins from plants: mechanism of action and food application. *Food Res Intern*. 2012;46:425-436.
20. Kawahara H. Characterizations of Functions of Biological Materials Having Controlling-Ability Against Ice Crystal Growth. In: Ferreira SO, ed. *Advanced Topics on Crystal Growth*. InTech; 2013:119-143.
21. Shalaev EY, Malakhov DV, Kanev AN, et al. Study of the phase diagram water fraction of the system water-glycine-sucrose by DTA and X-ray diffraction methods. *Thermochim Acta*. 1992;196:213-220.
22. Varshney DB, Kumar S, Shalaev EY, Kang S-W, Gatlin LA, Suryanarayanan R. Solute crystallization in frozen systems—use of synchrotron radiation to improve sensitivity. *Pharm Res*. 2006;23:2368-2374.
23. Surovtsev NV, Adichtchev SV, Malinovsky VK, et al. Glycine phases formed from frozen aqueous solutions: revisited. *J Chem Phys*. 2012;137. art. no. 065103.
24. Murray BJ, Bertram AK. Inhibition of solute crystallisation in aqueous H^+—$NH4^+$—$SO4^{2-}$ —H2O droplets. *Phys Chem Chem Phys*. 2008;10:3287-3301.
25. Ogienko AG, Boldyreva EV, Manakov A, et al. A new method of producing monoclinic paracetamol suitable for direct compression. *Pharm Res*. 2011;28:3116-3127.
26. Berejnov V, Husseini NS, Alsaied OA, Thorne RE. Effects of cryoprotectant concentration and cooling rate on vitrification of aqueous solutions. *J Appl Cryst*. 2006;39:244-251.
27. Dowell LG, Rinfret AP. Low temperature forms of ice as studied by x-ray diffraction. *Nature (London)*. 1960;188:1144-1148.
28. Thanatuksorn P, Kajiwara K, Murase N, Franks F. Freeze-thaw behaviour of aqueous glucose solutions-the crystallisation of cubic ice. *Phys Chem Chem Phys*. 2008;10:5452-5458.
29. Yagci YE, Antonietti M, Borner HG. Synthesis of Poly(tartar amides) as bioinspired antifreeze additives. *Macromol Rapid Commun*. 2006;27:1660-1664.
30. Baruch E, Mastai Y. Antifreeze properties of polyglycidol block copolymers. *Macromol Rapid Commun*. 2007;28:2256-2261.
31. Huang ML, Ehre D, Jiang Q, Hu C, Kirshenbaum K, Ward MD. Biomimetic peptoid oligomers as dual-action antifreeze agents. *Proc Natl Acad Sci U S A*. 2012;109:19922-19927.
32. Fitch AN. The high resolution powder diffraction beam line at ESRF. *J Res Natl Inst Stand Technol*. 2004;109:133-142.
33. Suryanarayanan R. Determination of the relative amounts of anhydrous—carbamazepine and carbamazepine dehydrate in a mixture by powder X-ray diffractometry. *Pharm Res*. 1989;6:1017-1024.
34. Roberts SNC, Williams AC, Grimsey IM, Booth SW. Quantitative analysis of mannitol polymorphs. X-ray powder diffractometry—exploring preferred orientation effects. *J Pharm Biomed Anal*. 2002;28:1149-1159.
35. Wright J, Vaughan G, Fitch A. *Merging data from a multi-detector continuous scanning powder diffraction system*. In: Commission on Crystallographic Computing International Union of Crystallography, Newsletter No. 1; 2003. Available at: http://www.iucr.org/iucr-top/comm/ccom/newsletters/. Accessed May 29, 2016.
36. Panagopoulou A, Kyritsis A, Sabater I, et al. Glass transition and dynamics in BSA—water mixtures over wide ranges of composition studied by thermal and dielectric techniques. *Biochim Biophys Acta*. 2011;1814:1984-1996.
37. Rasmussen DH, MacKenzie AP. Effect of solute on ice-solution interfacial free energy: calculation from measured homogeneous nucleation temperatures. In: Jellinek HHH, ed. *Water Structure at the Water-Polymer Interface*. New York: Plenum; 1971:126-145.
38. Michelmore RW, Franks F. Nucleation rates of ice in undercooled water and aqueous solutions of polyethylene glycol. *Cryobiology*. 1982;19:163-171.
39. Kanno H, Soga M, Kajiwara K. Linear relation between T_H (homogeneous ice nucleation temperature) and T_m (melting temperature) for aqueous solutions of sucrose, trehalose, and maltose. *Chem Phys Lett*. 2007;443:280-283.
40. Miyata K, Kann H. Supercooling behavior of aqueous solutions of alcohols and saccharides. *J Mol Liquids*. 2005;119:189-193.
41. Charoenrein S, Reid DS. The use of DSC to study the kinetics of heterogeneous and homogeneous nucleation of ice in aqueous systems. *Thermochim Acta*. 1989;156:373-381.
42. Ozilgen S, Reid DS. The use of DSC to study the effects of solutes on heterogeneous ice nucleation kinetics in model food emulsions. *Lebensm-Wiss-u-Technol*. 1993;26:116-120.
43. Koop T, Zobrist B. Parameterizations for ice nucleation in biological and atmospheric systems. *Phys Chem Chem Phys*. 2009;11:10839-10850.
44. Izmailov AF, Myerson AS, Arnold S. A statistical understanding of nucleation. *J Cryst Growth*. 1999;196:234-242.
45. MacKenzie AP. The physico-chemical basis for the freeze-drying process. *Dev Biol Stand*. 1977;36:51-57.
46. Goff HD, Verespej E, Jermann D. Glass transitions in frozen sucrose solutions are influenced by solute inclusions within ice crystals. *Thermochim Acta*. 2003;399:43-55.
47. Chang L, Milton N, Rigsbee D, et al. Using modulated DSC to investigate the origin of multiple thermal transitions in frozen 10% sucrose solutions. *Thermochim Acta*. 2006;444:141-147.
48. Corti HR, Angell CA, Auffret T, et al. Emperical and theoretical models of equilibrium and non-equilibrium transition temperatures of supplemented phase diagrams in aqueous systems (IUPAC Technical Report). *Pure Appl Chem*. 2010;82:1065-1097.
49. Levine H, Slade L. A polymer physico-chemical approach to the study of commercial starch hydrolysis products (SHPs). *Carbohydr Polym*. 1986;6:213-244.
50. Rasmussen D, Luyet B. Complementary study of some non-equilibrium phase transitions in frozen solutions of glycerol, ethylene glycol, glucose and sucrose. *Biodynamica*. 1969;10:319-331.
51. Roos Y, Karel M. Water and molecular weight effects on glass transitions in amorphous carbohydrates and carbohydrate solutions. *J Food Sci*. 1991;56:1676-1681.
52. Shalaev EY, Franks F. Structural glass transitions and thermophysical processes in amorphous carbohydrates and their supersaturated solutions. *J Chem Soc Faraday Trans*. 1995;91:1511.
53. Wu J, Reading M, Craig DQM. Application of calorimetry, sub-ambient atomic force microscopy and dynamic mechanical analysis to the study of frozen aqueous trehalose solutions. *Pharm Res*. 2008;25:1396-1404.
54. Ablett S, Izzard MJ, Lillford PJ. Differential scanning calorimetric study of frozen sucrose and glycerol solutions. *J Chem Soc Faraday Trans*. 1992;88:789-794.
55. Bogdan A, Molina MJ, Tenhu H, Bertel E, Bogdan N, Loerting T. Visualization of freezing process in situ upon cooling and warming of aqueous solutions. *Sci Rep*. 2014;4:7414.
56. Bogdan A, Molina MJ, Tenhu H, Loerting T. Multiple glass transitions and freezing events of aqueous citric acid. *J Phys Chem A*. 2015;119:4515-4523.
57. Salnikova M, Varshney D, Shalaev E. Heterogeneity of protein environments in frozen solutions and in the dried state. In: Varshney D, Singh M, eds. *Lyophilized Biologics and Vaccines: Modality-Based Approaches*. New York, Heidelberg, Dordrecht, London: Springer; 2015.
58. Varshney DB, Elliott JA, Gatlin LA, Kumar S, Suryanarayanan R, Shalaev EY. Synchrotron x-ray diffraction investigation of the anomalous behavior of ice during freezing of aqueous systems. *J Phys Chem B*. 2009;113:6177-6182.
59. Gekko K, Satake I. Differential scanning calorimetry of unfreezable water in water-protein-polyol systems. *Agric Biol Chem*. 1981;45:2209-2217.
60. Angell CA. The old problems of glass and the glass transition, and the many new twists. *Proc Natl Acad Sci U S A*. 1995;92:6675-6682.
61. Powder Diffraction File PDF Card #016-0687.
62. Jenkins R, Snyder RL. *Introduction to Powder X-ray Diffractometry. Chemical Analysis: A Series of Monographs on Analytical Chemistry and Its Applications*. Vol. 138. New York, Chichester, Brisbane, Toronto, Singapore: John Wiley & Sons; 1996:17.
63. Alexander L, Klug HP. Basic aspects of x-ray absorption in quantitative diffraction analysis of powder mixtures. *Anal Chem*. 1948;20:886-889.
64. Siniti M, Jabrane S, Letoffe JM. Study of the respective binary phase diagrams of sorbitol with mannitol, maltitol and water. *Thermochim Acta*. 1999;325:171-180.
65. Predel B, Hoch M, Pool M. *Phase Diagrams and Heterogeneous Equilibria*. Berlin, Heidelberg: Springer-Verlag; 2004:29.
66. Snell EH, Bellamy HD, Rosenbaum G, van der Woer MJ. Non-invasive measurement of X-ray beam heating on a surrogate crystal sample. *J Synchrotron Radiat*. 2007;14:109-115.
67. Schroder S, Reichert H, Schroder H, et al. Radiation-induced premelting of ice at silica interfaces. *Phys Rev Lett*. 2009;103:095502.
68. Shalaev E, Soper AK. Water in a “soft” confining media: structure of water in amorphous sorbitol. *J Phys Chem Lett*. 2016 [In preparation].
69. Uchida T, Takeya S. Powder X-ray diffraction observations of ice crystals formed from disaccharide solutions. *Phys Chem Chem Phys*. 2010;12:15034-15039.
70. Malkin TL, Murray BJ, Brukhno AV, Anwar J, Salzmann CG. Structure of ice crystallized from supercooled water. *Proc Natl Acad Sci U S A*. 2012;109:1041-1045.
71. Delhez R, de Keijser TH, Langford JI, Louër D, Mittemeijer EJ, Sonneveld EJ. Crystal imperfection broadening and peak shape in the Rietveld method. In: Young RA, ed. *The Rietveld Method (IUCr Monograph on Crystallography, No. 5*. Oxford: International Union of Crystallography/Oxford University Press; 1995:132-166.
72. Balzar D. X-ray diffraction line broadening: modeling and applications to high-Tc superconductors. *J Res Natl Inst Stand Technol*. 1993;98:321-353.
73. Williamson GK, Hall WH. X-ray line broadening from filed aluminium and wolfram. *Acta Metall*. 1953;1:22-31.

74. Gibson MI. Slowing the growth of ice with synthetic macromolecules: beyond antifreeze(glyco) proteins. *Polym Chem*. 2010;1:1141-1152.
75. Czechura P, Tam RY, Dimitrijevic E, Murphy AV, Ben RN. The importance of hydration for inhibiting ice recrystallization with C-linked antifreeze glycoproteins. *J Am Chem Soc*. 2008;130:2928-2929.
76. Petrenko VF, Whitworth RW. *Physics of Ice*. Oxford: Oxford University Press; 1999:227-251.
77. Elbaum M, Lipson SG, Dash JG. Optical study of surface melting on ice. *J Cryst Growth*. 1993;129:491-505.
78. Hew CL, Yang DSC. Protein interaction with ice. *Eur J Biochem*. 1992;203:33-42.
79. Raymoind JA, DeVries AL. Adsorption inhibition as a mechanism of freezing resistance in polar fishes. *Proc Natl Acad Sci U S A*. 1977;74:2589-2593.
80. Kuiper MJ, Lankin C, Gauthier SY, Walker VK, Davies PL. Purification of antifreeze proteins by adsorption to ice. *Biochem Biophys Res Commun*. 2003;300:645-648.
81. Webb SD, Golledge SL, Cleland JL, Carpenter JF, Randolph TW. Surface adsorption of recombinant human interferon gamma in lyophilized and spray-lyophilized formulations. *J Pharm Sci*. 2002;91:1474-1487.
82. Abdul-Fattah AM, Lechuga-Ballesteros D, Kalonia DS, Pikal MJ. The impact of drying method and formulation on the physical properties and stability of methionyl human growth hormone in the amorphous solid state. *J Pharm Sci*. 2008;97:163-184.
83. Strambini GB, Gabellieri E. Protein stability in ice. *Biophys J*. 2007;92:2131-2138.
84. Reid D, Kerr WL, Zhao J, Wada Y. *Surface energy at the ice-solution interface for systems containing antifreeze biopolymers*. Special Publication. In: *Food Macromolecules and Colloids*. 156. London: Royal Society of Chemistry; 1995:141-145.